Microelectronic Engineering 119 (2014) 122–126

Contents lists available at ScienceDirect

Microelectronic Engineering

journal homepage: www.elsevier.com/locate/mee

Fabrication and characterization of combined metallic nanogratings and ITO electrodes for organic photovoltaic cells

D.A. Gollmer [a,*,1], F. Walter [a,1], C. Lorch [a], J. Novák [a,b], R. Banerjee [a], J. Dieterle [a], G. Santoro [c], F. Schreiber [a], D.P. Kern [a], M. Fleischer [a,*]

[a] Institute for Applied Physics and Center LISA+, Eberhard Karls Universität Tübingen, Auf der Morgenstelle 10, 72076 Tübingen, Germany
[b] Central European Institute of Technology, Masaryk University, Kamenice 5, CZ-62500 Brno, Czech Republic
[c] HASYLAB at DESY, Notkestraße 85, 22607 Hamburg, Germany

ARTICLE INFO

Article history:
Received 29 October 2013
Received in revised form 9 March 2014
Accepted 27 March 2014
Available online 5 April 2014

Keywords:
Plasmonic solar cells
Plasmonic nanogratings
Nano imprint lithography
Extinction spectroscopy
Organic photovoltaics
GISAXS

ABSTRACT

Organic photovoltaic devices are interesting alternatives to conventional silicon based photovoltaic cells, due to potentially lower material costs and energy consumption during the fabrication process. However, the energy conversion efficiency of organic photovoltaic cells may still be improved. One possible approach is a combination with metallic nanostructures to improve light absorption properties in the active layer. We report on the fabrication and characterization of metallic nanogratings integrated with an indium tin oxide (ITO) electrode to be combined with small-molecule organic photovoltaic cells. With respect to geometry and extinction properties gratings fabricated by two different fabrication methods, conventional electron beam lithography and nanoimprint lithography, are presented. Furthermore, gratings fabricated on top of ITO are compared to gratings integrated both below and within ITO electrodes. Fabricating structures below or within electrodes is advantageous for organic thin film techniques to avoid compromising the crystallinity of the organic thin film and short-circuiting across the thin layer.

1. Introduction

Organic photovoltaic (OPV) cells are a cost and energy efficient alternative to conventional silicon based devices. However, OPV cells still have a low energy conversion efficiency compared to established solar cells [1]. The efficiency of an OPV cell can be expressed as the product of the internal efficiencies of (i) photon absorption and formation of an exciton, (ii) exciton diffusion to the organic–organic interface, (iii) dissociation of the exciton and formation of an electron–hole polaron pair, and (iv) finally charge collection and extraction [2]. Since the exciton diffusion lengths are in the range of several tens of nanometers [3,4], increasing the thickness of the organic film system for better light harvesting does not necessarily improve the efficiency of such devices. As a possible way to increase the absorption cross-section, but retaining the thickness of the organic matrix of these cells, the use of metallic nanostructures has recently been suggested and reviewed [1,5]. Metallic nanostructures, nanostructured electrodes or nanoparticles have already been used in inorganic and organic photovoltaic cells to improve their efficiencies [1,5]. The incorporation of metallic nanoparticles or nanostructures has been successfully realized at the front electrode [6,7], within the active layer [8] or at the back electrode [9]. The influence of metallic nanostructures on the efficiency of solar cells has also been studied in simulations [10,11].

Here we present fabrication methods of gratings on top of, within or below the transparent front indium tin oxide (ITO) electrode that will subsequently be combined with small molecule organic photovoltaic cells (Fig. 1c). The organic film system is evaporated in a UHV-chamber (ultra high vacuum) [12]. Diindenoperylene (DIP) and C_{60} are targeted, which have been shown to present an attractive combination [13]. For hybrid combinations of metallic nanostructures at the front electrode and organic thin film photovoltaic devices two challenges need to be met: first, a large-scale fabrication method for nanostructures is necessary for fabricating cells in a cost effective way and with high throughput, second, undesired effects that the additional topography may have on the organic thin film system have to be minimized. Surface roughness at the front electrode and the combination of different materials, *i.e.*, ITO and Au can influence the organic thin film system [14–16]. The height modulation of the nanostructures may cause short-circuits in organic thin film devices. In addition, the nanograting may decrease the crystallinity of the organic thin films, which can reduce the exciton diffusion length and the charge carrier

* Corresponding authors. Tel.: +49 70712974528.
E-mail addresses: dominik.gollmer@uni-tuebingen.de (D.A. Gollmer), monika.fleischer@uni-tuebingen.de (M. Fleischer).
[1] These authors contributed equally to this work.

http://dx.doi.org/10.1016/j.mee.2014.03.042
0167-9317/

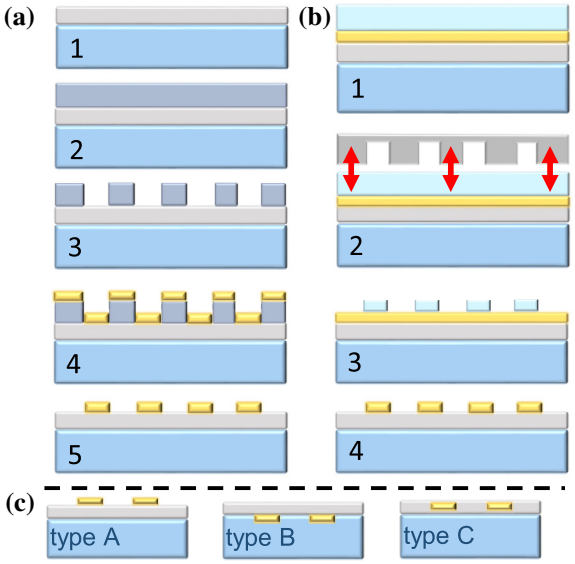

Fig. 1. (a) Fabrication scheme of nanogratings on ITO electrodes with EBL: (1) ITO/glass substrate, (2) PMMA spin-coating, (3) EBL and development, (4) evaporation of Au and (5) lift-off. (b) Fabrication of gratings by UV-NIL: (1) glass/ITO electrode with Au film and imprint resist, (2) imprint step, (3) resist mask after oxygen plasma, (4) ion-milling. (c) Schematic of the three sample types: (type A) nanowires on ITO, (type B) nanowires below ITO, (type C) nanowires embedded in ITO.

mobility in the organic film system [17,18]. To address potential large-scale fabrication, UV nanoimprint lithography (UV-NIL) is evaluated for the fabrication of nanogratings. The results are compared to gratings fabricated by electron beam lithography (EBL). To circumvent the problem of extra topography, structures can be fabricated below or embedded within the ITO electrode. Corresponding fabrication methods are established and presented here. The different fabrication methods and the location of the nanostructures (on, within or below the electrode) can influence the optical properties and need to be thoroughly investigated. Therefore, a model system consisting of gold nanowire gratings with wire widths of several tens of nanometers up to ~150 nm and periods of 400–700 nm are fabricated with EBL and UV-NIL at different locations within the glass/ITO substrate. The geometrical properties are examined by scanning electron microscopy (SEM), atomic force microscopy (AFM) and grazing-incidence small-angle X-ray scattering (GISAXS) [19]. The optical properties of the structures are investigated by white-light extinction spectroscopy.

2. Methods

2.1. Fabrication processes

Two methods for fabricating gold nanogratings were used. On the one hand the structures were fabricated via electron beam lithography and on the other hand, as EBL is quite time consuming, nanoimprint lithography was used. All the gratings were made of gold, as it has good plasmonic properties and does not oxidize easily when exposed to air. The thickness of the Au structures was nominally 20 nm. Resulting gratings with a comparable period (~600 nm each) and widths (71–87 nm) are shown in Fig. 2a–d. Via EBL, structures were fabricated on top of, within and below an ITO electrode (Figs. 1c and 2a, c, d). For the fabrication of gratings on ITO electrodes (Fig. 2a) first a ~50 nm thick ITO film

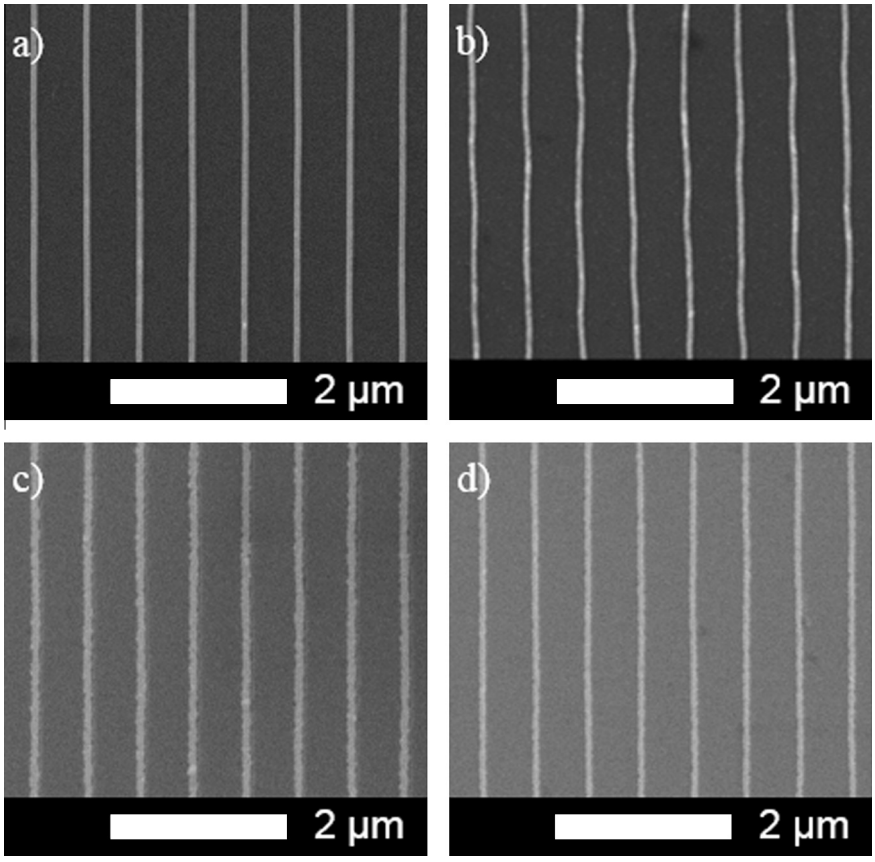

Fig. 2. (a and b) SEM images of type A gratings fabricated by (a) EBL (period: 605 ± 1 nm, width: 71 ± 2 nm) and (b) UV-NIL (period: 606 ± 2 nm, width: 73 ± 9 nm). (c) Type B grating (period: 607 ± 1 nm, width: 87 ± 2 nm) and (d) type C grating (period: 606 ± 1 nm, width: 76 ± 2 nm), (c and d) both fabricated by EBL.

was sputtered onto a cleaned glass substrate by magnetron sputtering (20 W, $3 * 10^{-3}$ mbar). Then a PMMA (Poly (methyl methacrylate)) film (thickness ~ 220 nm) was spin-coated onto the ITO, and exposed via EBL (Philips XL30, 30 kV). After developing the exposed resist (1:3, Methyl isobutyl ketone (MIBK): Isopropyl alcohol (IPA), 75 s), 20 nm gold was thermally evaporated under high vacuum (HV) conditions, followed by lift-off in acetone. The height profile of the final wires is shown in Fig. 3d. Gold gratings with different periods and widths were fabricated this way.

As EBL is a time consuming serial process, a parallel process of UV-NIL was also used to fabricate gratings on ITO electrodes (Figs. 1b and 2b) [20–22]. In contrast to EBL the resist structures to be used as etch masks were not generated by a patterned exposure, but by mechanical transfer of the pattern from a stamp. To this effect a stamp was pressed into the liquid resist, which was then cross-linked by a blanket UV exposure. For the stamp preparation first a silicon master was fabricated. PMMA was spin-coated onto a silicon wafer and patterned via EBL. Aluminum was deposited by electron beam evaporation under HV conditions and lifted off. The aluminum pattern was then used as a mask for reactive ion etching of the silicon (Oxford Instruments, 100 W, 60 mTorr, 15 sccm CHF_3, 15.6 sccm SF_6, 24 sccm O_2, 60 s) and afterwards removed by a weak base (developer ma-D 331 by micro resist technology). After applying an anti-sticking layer of tridecafluoro-(1,1,2,2-tetrahydrooctyl)-trichlorosilane (F13-TCS) the master could be used as a mold for the fabrication of a working stamp. To this effect a drop of OrmoStamp (micro resist technology) was deposited on the master, and a clean glass substrate was placed onto it. The evenly distributed polymer was prebaked (10 min, 80 °C) and exposed to UV light, followed by a post exposure bake (15 min, 130 °C). After separation from the master and coating with another anti-sticking layer, this stamp could be used for several imprint cycles. For the grating fabrication a UV-sensitive resist (UVcur21 by micro resist technology) was spin-coated onto a glass substrate with a 50 nm ITO and a 20 nm gold layer. The stamp was pressed into the liquid resist, and the stack was exposed by UV light, cross-linking the resist. A residual resist layer still covering the whole substrate after separation was removed via reactive ion etching with oxygen. The imprint resist could then be used as an etching mask in an argon ion milling process (U_{beam} = 300 V, $7.4 * 10^{-4}$ mbar, 50 s). Residuals of the imprint resist were removed again by an oxygen plasma step.

The structures prepared below the ITO electrode were embedded into the glass substrate using EBL (Figs. 2c and 3b). For the fabrication of these gratings PMMA (~440 nm) was spin-coated onto a clean glass substrate in a two layer process, and an aluminum film was evaporated on top to obtain a conducting surface for EBL. After the electron beam exposure the aluminum was removed by ma-D 331 (micro resist technology), and the PMMA was developed (1:3, MIBK:IPA, 75 s). The PMMA film was then used as a mask in a reactive ion etching process (Oxford Instruments, 122 W, 79 mTorr, 40 sccm CHF_3, 1.4 sccm N_2, 56 s). After this step gold (20 nm) was evaporated onto the sample, and after the lift off process only the gold within the etched channels remained. AFM measurements confirmed a much reduced overall surface roughness (~9 nm peak-to-peak, Fig. 3e) compared to the sample with structures on ITO/glass substrate, which might be reduced further by continued optimization. Finally an ITO film with ~20 nm was sputtered onto the sample.

For the fabrication of the gratings embedded in ITO (Figs. 2d and 3c), a clean glass substrate was sputtered again with ITO (film thickness ~50 nm), onto which PMMA was spin-coated (~220 nm). After EBL, the PMMA pattern was used as an etching mask for an argon milling process (U_{beam} = 300 V, $7.4 * 10^{-4}$ mbar, 85 s) to transfer the gratings into the ITO electrode. Then gold was evaporated onto the sample, and after the lift off process only the gold within the etched channels was left. AFM measurements confirmed a nearly planar surface (surface roughness ~ 3 nm, Fig. 3f).

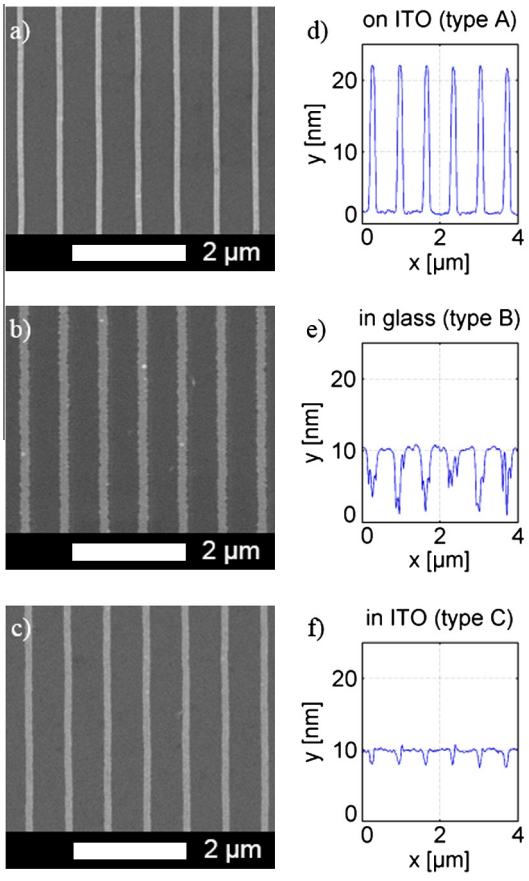

Fig. 3. In the left column (a–c) SEM images of gratings and in the right column (d–f) AFM cross-sections of the corresponding gratings are shown. (a and d) type A grating (period: 706 ± 1 nm, width: 98 ± 1 nm), height: ~20 nm, (b and f) type B grating before ITO sputtering (period: 709 ± 2 nm, width: 145 ± 5 nm), roughness: ~9 nm, (c and f) type C grating (period: 707 ± 2 nm, width: 122 ± 2 nm), roughness: ~3 nm.

2.2. Geometrical properties

The geometry of the nanowire gratings (wire width, period) was investigated by SEM (Figs. 2 and 3a–c), and the roughness of the electrode surface was investigated by AFM (Fig. 3d–f). Additional gratings were fabricated by EBL on a silicon substrate for GISAXS measurements (height of the structures 3 nm Ti plus 12 nm Au, Fig. 4). The sample fabricated for GISAXS measurements consisted of a 10 × 3 array of nano-gratings with edge dimensions of

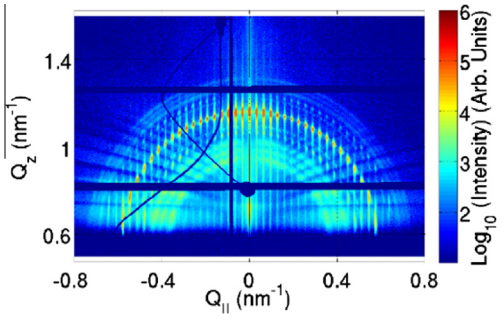

Fig. 4. GISAXS image of a sample with a 10 × 3 array of nano-gratings (period: 196 ± 2 nm, width: 53 nm) on silicon substrate.

$100 \times 100\ \mu m^2$ each, wire-to-wire nominal distance (period) of 200 nm, and a wire width of ~50 nm. GISAXS provides statistically relevant information on the large structured area of the sample. The array of nanogratings leads to a high signal to noise ratio in the scattering pattern. The method was used to verify the large-scale quality of the structures and the calibration of the SEM measurements. The nominal wire period of only 200 nm was chosen to fit the resolution of the scattering experiment, since the distance of the interference fringes of scattered X-rays is inversely proportional to the wire distance. GISAXS was measured at the P03/MiNaXS beamline of the high brilliance PETRA III synchrotron (Hamburg, Germany) [23] using an X-ray energy of 11.4 keV. The primary X-ray beam impinged on the sample at a grazing angle of 0.60°, and the wires were oriented parallel to the incidence plane. The GISAXS image was collected using a PILATUS 1 M detector at a distance of 4900 mm from the sample.

2.3. Extinction measurements

For extinction measurements an inverted microscope was used (Nikon Ti-U). The samples with the nanowire gratings on top were illuminated by a nearly collimated white light beam (halogen lamp) from above. The transmitted light was detected through an objective (20×) with a numerical aperture of 0.5. A pinhole with a diameter of 200 μm in the image plane was used for spatial filtering. With this filter just the light of a disk with a diameter of about 10 μm in the object plane was coupled into a spectrometer. As a reference spectrum the light transmitted through the substrate was used. Both the reference spectrum and the spectrum transmitted through the structured area of the sample were corrected for the dark current of the CCD detector of the spectrometer. From the corrected spectra I_{ref} and $I_{grating}$ the extinction spectrum I_{ext} could be calculated to: $I_{ext} = (I_{ref} - I_{grating})/I_{ref}$.

3. Results and discussion

The SEM images (Fig. 2) show regular gratings for both fabrication methods of structures on ITO, EBL and UV-NIL (Fig. 2a and b), as well as for structures below and embedded in ITO (Fig. 2c and d). The edge roughness is low, only the structures below ITO embedded in glass show an increased edge roughness and residuals of the lift-off process, possibly due to slanted sidewalls in the resist as a result of the etching process. The AFM line scan in Fig. 3d shows gold lines on ITO with a height of ~20 nm. AFM measurements on gratings embedded in glass, before sputtering ITO, and on gratings embedded within ITO show much reduced topographical features (Fig. 3e and f). The peak-to-peak roughness of the structures in glass before sputtering ITO is about 9 nm (Fig. 3e), the peak-to-peak roughness of structures within ITO is only about 3 nm (Fig. 3f), compared to a structure height of the gold lines, corresponding to the etch depth, of nominally 20 nm. By fabricating structures below and within ITO thus deterioration of the crystal structure of organic films through modulation of the surface shape can be reduced. Changes in the crystallinity through the alternating materials of substrate and wires can be prevented by fabricating the wires below ITO electrodes.

GISAXS measurements were performed for structures on silicon substrates to calibrate the periodicity of the grating and to monitor the homogeneity of the gratings described in Section 2.2. Fig. 4 shows a GISAXS image of the nanogratings displaying a series of vertical lines, also known as grating truncation rods (GTRs) [24]. The lateral distance of the GTRs is $\Delta Q_{||}=2\pi/D$, where $Q_{||}$ is the in-plane component of the momentum transfer vector, and D is the distance of the wires. The arc of the most intense spots corresponds to the intersections of the GTRs with the Ewald sphere [24]. The existence of the single arc evidences good parallel alignment of gold lines even between the different nanogratings of the 10 × 3 array. According to this measurement the periodicity of the wires is $D = 196 \pm 2$ nm, which is in good agreement with the nominal periodicity of 200 nm.

Optical properties of 1D or 2D plasmonic nanogratings have been investigated theoretically [25,26] and experimentally [27–29] under different aspects. Here the optical properties of gratings fabricated by EBL and UV-NIL and of gratings fabricated on, below and within ITO electrodes by EBL were compared. Fig. 5a and b shows optical extinction spectra of gold gratings on ITO fabricated by EBL (red curves) and UV-NIL (green curves) for periods of ~500 nm and ~600 nm and different wire widths. In Fig. 5c and d the extinction spectra of gratings on ITO (red curves), gratings embedded in glass without ITO (dark blue curves) and below an about 20 nm thick ITO film (bright blue curves) are shown together with spectra of gratings in the ITO film (yellow curves), for periods of ~500 nm (5c) and ~700 nm (5d) each. Extinction spectra on ITO substrates (Fig. 5a and b) show plasmon resonances which redshift with increasing wire widths, while the extinction intensity rises for larger wire widths as expected. This size dependence of the plasmon resonance and extinction cross section is extensively discussed in the literature [30,31]. Compared to the plasmon resonances of the gratings fabricated by EBL on ITO, the resonances of the gratings fabricated by UV-NIL are clearly redshifted for comparable periods and wire widths (Fig. 5a and b). This effect can be attributed to different aspect ratios (height:width) of the respective wires. While the structure height of the gratings fabricated by EBL was exactly determined to 20 nm, the geometry of the gratings fabricated by UV-NIL may differ from the nominal gold layer thickness due to overetching during the etch mask transfer or mask removal. By changing the aspect ratio of the structures, the plasmon resonance can be strongly influenced [32]. The height of the structures was verified by AFM measurements. For the structures fabricated by UV-NIL, a height of about 10 nm was determined. This reduced aspect ratio of the wires can explain the redshift [32]. Comparing Fig. 5a and b, the position of the resonances is very little influenced by the grating period.

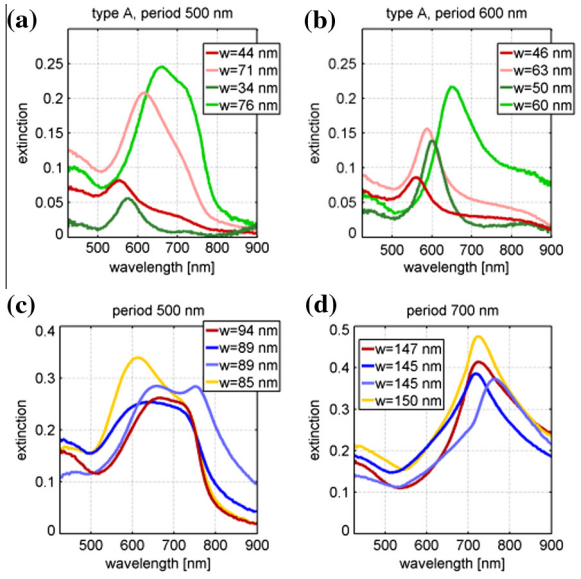

Fig. 5. (a and b) extinction spectra of type A nanowire gratings (red curves: EBL, green curves: NIL), with (a) period 500 nm, (b) period 600 nm, and different wire widths; (c and d) extinction spectra of type A (EBL) gratings (red curves), type B gratings (dark blue curves: without ITO, bright blue curves: with ITO) and type C gratings (yellow curves) for a comparable period of (c) ~500 nm, (d) ~700 nm and widths of (c) ~90 nm, (d) ~150 nm. (For the references to color in this figure legend, the reader is referred to the online version of this article.)

For some of the gratings a second, grating-induced mode can also be observed, which has been discussed in the literature as well [25,27,29,33,34]. For the gratings presented here, it occurs in the wavelength region where the first grating order on the substrate side radiates under grazing angle (almost 90°) [29,34]. For perpendicular illumination this is the case when the wavelength in the glass substrate (n_{glass} = 1.5) is comparable to the period of the wires. This mode is e.g. clearly visible for gratings with a period of 500 nm (Fig. 5a and c) at ~730 nm.

Plasmonic nanogratings fabricated by EBL below or embedded in ITO as well as gratings on top of ITO show resonances in the same wavelength region for similar grating parameters (Fig. 5c and d). The resonances in the ~500 nm and ~700 nm period extinction spectra of the gratings in glass before (dark blue) and after sputtering an ITO film onto the gratings (bright blue) show a redshift. This shift can be explained by the higher effective refractive index above the grating (n_{air} = 1.0, n_{glass} = 1.5, n_{ITO} = 1.88 at a wavelength of 600 nm [35]), as can the redshift of the grating-induced mode.

As Fig. 5 shows, the wavelength position of the resonance can easily be tuned by the geometry of the gratings. This tunability of the resonance is a further advantage of the plasmonic gratings, since it can thus be matched to the HOMO–LUMO transition bands of organic semiconductors to optimize interaction between the two system components.

4. Conclusion

We compared the properties of Au nanowire gratings fabricated by serial electron beam lithography and parallel UV-NIL on ITO electrodes. Fabricating these structures with a parallel fabrication method such as UV-NIL is interesting for integrating them in thin film photovoltaic cells, due to the potentially high throughput of this technique. To avoid additional surface topography due to the nanogratings, which could be problematic for thin film photovoltaic configurations, or material influence of the grating on the crystallinity of the thin film material, methods for fabricating these structures below and within ITO electrodes were established. The geometrical properties were studied by SEM, AFM and GISAXS. Furthermore the optical properties, especially the plasmon mode and the grating-induced mode, were investigated by extinction spectroscopy. The optical properties of gratings with similar grating parameters fabricated by EBL and UV-NIL were compared, as well as the optical properties of gratings with nearly the same grating parameters of the three different grating types A (on ITO), B (in glass below ITO) and C (in ITO). The observed resonance shifts can be explained by differences in the detailed geometry of the metal wires and the different dielectric environments for the three grating types. In future the parallel fabrication method can be extended to gratings below and within ITO electrodes.

Acknowledgements

Financial support by the Baden-Württemberg Foundation in the program "Organic Photovoltaics and Dye Sensitized Solar Cells" and provision of beam-time at the PETRA III (HASYLAB, Hamburg) synchrotron facility are gratefully acknowledged. C.L. received financial support from the Carl-Zeiss-Stiftung. J.N. was supported by the project CEITEC (CZ.1.05/1.1.00/02.0068) from the European Regional Development Fund and by the EC 7th Framework Programme (286154/SYLICA).

References

[1] Q. Gan, F.J. Bartoli, Z.H. Kafafi, Adv. Mater. 25 (2013) 2385–2396.
[2] S.R. Forrest, MRS Bull. 30 (2005) 28–32.
[3] D. Kurrle, J. Pflaum, Appl. Phys. Lett. 92 (2008) 1333061–1333063.
[4] P. Peumans, A. Yakimov, S.R. Forrest, J. Appl. Phys. 93 (2003) 3693–3723.
[5] H.A. Atwater, A. Polman, Nat. Mater. 9 (2010) 865.
[6] D. Derkacs, S.H. Lim, P. Matheu, W. Mar, E.T. Yu, Appl. Phys. Lett. 89 (2006) 0931031–0931033.
[7] S.-S. Kim, S.-I. Na, J. Jo, D.-Y. Kim, Y.-C. Nah, Appl. Phys. Lett. 93 (2008) 0733071–0733073.
[8] B.P. Rand, P. Peumans, S.R. Forrest, J. Appl. Phys. 96 (2004) 7519–7526.
[9] K. Tvingstedt, N.-K. Persson, O. Inganäs, A. Rahachou, I.V. Zozoulenko, Appl. Phys. Lett. 91 (2007) 1135141–1135143.
[10] V.E. Ferry, L.A. Sweatlock, D. Pacifici, H.A. Atwater, Nano Lett. 8 (2008) 4391–4397.
[11] R.A. Pala, J. White, E. Barnard, J. Liu, M.L. Brongersma, Adv. Mater. 21 (2009) 3504–3509.
[12] A. Hinderhofer, F. Schreiber, ChemPhysChem 13 (2012) 628–643.
[13] J. Wagner, M. Gruber, A. Hinderhofer, A. Wilke, B. Bröker, J. Frisch, P. Amsalem, A. Vollmer, A. Opitz, N. Koch, F. Schreiber, W. Brütting, Adv. Funct. Mater. 20 (2010) 4295–4303.
[14] A. Schöll, F. Schreiber, Chapter 26 – Thin Films of Organic Molecules: Interfaces and Epitaxial Growth, Molecular Beam Epitaxy, Elsevier, Oxford, 2013. pp. 591–609.
[15] A.C. Dürr, F. Schreiber, M. Münch, N. Karl, B. Krause, V. Kruppa, H. Dosch, Appl. Phys. Lett. 81 (2002) 2276–2278.
[16] A.C. Dürr, N. Koch, M. Kelsch, A. Rühm, J. Ghijsen, R.L. Johnson, J.J. Pireaux, J. Schwartz, F. Schreiber, H. Dosch, A. Kahn, Phys. Rev. B 68 (2003) 1154281–11542812.
[17] L. Zhou, X.-F. Wang, Q. Han, J.-C. Wu, Z.-Y. Li, Appl. Phys. Lett. 96 (2010) 633011–633013.
[18] D. Knipp, R.A. Street, A. Völkel, J. Ho, J. Appl. Phys. 93 (2003) 347–355.
[19] G. Renaud, R. Lazzari, F. Leroy, Surf. Sci. Rep. 64 (2009) 255–380.
[20] S.Y. Chou, P.R. Krauss, P.J. Renstrom, Appl. Phys. Lett. 67 (1995) 3114–3116.
[21] J. Haisma, M. Verheijen, K. van den Heuvel, J. van den Berg, J. Vac. Sci. Technol. B 14 (1996) 4124–4128.
[22] R. Löffler, M. Fleischer, D.P. Kern, C. Matschegewski, S. Stahlke, B. Nebe, R. Lange, J. Vac. Sci. Technol. B 30 (2012). 06F901-1–06F901-5.
[23] A. Buffet, A. Rothkirch, R. Döhrmann, V. Körstgens, M.M. Abul, J. Synchrotron Radiat. 19 (2012) 647–653.
[24] P. Mikulík, M. Jergel, T. Baumbach, E. Majková, E. Pincík, S. Luby, L. Ortega, R. Tucoulou, P. Hudek, I. Kostic, J. Phys. D: Appl. Phys. 34 (2001) A188–A192.
[25] M. Meier, A. Wokaun, P.F. Liao, J. Opt. Soc. Am. B 2 (1985) 931–949.
[26] L. Zhao, K.L. Kelly, G.C. Schatz, J. Phys. Chem. B 107 (2003) 7343–7350.
[27] B. Lamprecht, G. Schider, R.T. Lechner, H. Ditlbacher, J.R. Krenn, A. Leitner, F.R. Aussenegg, Phys. Rev. Lett. 84 (2000) 4721–4724.
[28] G. Schider, J.R. Krenn, W. Gotschy, B. Lamprecht, H. Ditlbacher, A. Leitner, F.R. Aussenegg, J. Appl. Phys. 90 (2001) 3825–3830.
[29] A. Christ, T. Zentgraf, J. Kuhl, S.G. Tikhodeev, N.A. Gippius, H. Giessen, Phys. Rev. B 70 (2004) 1251131–12511315.
[30] G. Mie, Ann. Phys. 330 (1908) 377–445.
[31] U. Kreibig, M. Vollmer, Optical Properties of Metal Clusters, Springer, Berlin Heidelberg, 1995.
[32] H. Kuwata, H. Tamaru, K. Esumi, K. Miyano, Appl. Phys. Lett. 83 (2003) 4625–4627.
[33] C.L. Haynes, A.D. McFarland, L. Zhao, R.P. Van Duyne, G.C. Schatz, L. Gunnarsson, J. Prikulis, B. Kasemo, M. Käll, J. Phys. Chem. B 107 (2003) 7337–7342.
[34] N. Felidj, G. Laurent, J. Aubard, G. Levi, A. Hohenau, J.R. Krenn, F.R. Aussenegg, J. Chem. Phys. 123 (2005) 221103–221105.
[35] Sopra n&k Database (Sopralab, 2012) <www.sopra-sa.com>.